Electronic structure of the (111) surface of semiconductors*

S. Ciraci, I. P. Batra, and W. A. Tiller†
IBM Research Laboratory, San Jose, California 95193
(Received 12 May 1975)

The electronic structure of the (111) surface of semiconductors is investigated using the bond-orbital model. The semi-infinite solid is represented by a system which has the two-dimensional periodicity of the (111) surface, but the third dimension is terminated after a finite number of layers, which leads to a convergent electronic band structure. Since there is an abundance of experimental data on Si(111), we have examined this material in great detail. The total densities of states and the energy-band structures are presented for ideal, relaxed, and (2×1) reconstructed Si(111). The effect of the reconstruction is to split the universal surface states, S_1, S_2, and S_3, into various bands. In particular, we have been able to explain various features of the recent angular resolved photoemission from cleaved Si(111) without invoking any new surface states. The calculated electronic structure of ideal Ge(111) and diamond (111) is briefly discussed. The chemisorption of hydrogen on Si(111) is also studied. The surface states of the compound semiconductors, e.g., AlP are found to have similar features to the elemental semiconductors. However, their energy locations depend on the nature of the surface (i.e., anion or cation type). We compare our results with photoemission experiments.

I. INTRODUCTION

Current advances in capabilities to measure precise surface properties have stimulated many experimental and theoretical studies in this area. The surface electronic properties of semiconductors, whose bulk properties are fairly well known, have been the focus of much recent attention. The early pioneering work of Tamm[1] and Schockley[2] clearly established that the breakdown of the crystalline periodicity due to the presence of a surface, leads to new states designated as intrinsic surface states. Many sophisticated treatments for a detailed understanding of surface states have appeared subsequently.[3–12]

Most recently, interest in the study of the electronic structure of semiconductor surfaces has been brought about by various spectroscopic measurements which are now available. Photoelectric measurement of Allen and Gobelli[13] and of Fischer and Eden[14] first revealed photoemission from surface states. Later, Eastman and Grobman[15] and Wagner and Spicer[16] observed the surface states near the valence-band edge. Electron-energy-loss and photoemission studies of Rowe and Ibach[17] brought to attention additional intrinsic surface states. Almost simultaneously Appelbaum and Hamann[8] reported the first self-consistent calculation of intrinsic surface states for both ideal (unrelaxed-unreconstructed) and relaxed Si(111)-(1×1) surfaces.

In this paper, we present a detailed study of the (111) surface electronic structure of semiconductors in the diamond and sphalerite structures by using the bond-orbital model[18,19] (BOM). The use of bond orbitals[20] rather than atomic orbitals allows one to work with the fcc structure rather than the diamond or sphalerite structure. Therefore, energy-band structure plus total and local densities of states can be calculated using relatively few energy parameters. Unlike some previous implementations of tight-binding methods for surface calculations,[9] the above energy parameters in the BOM are obtained strictly from bulk calculations without appealing to any other surface calculations. Furthermore, in the bond picture it is straightforward to examine various models of reconstruction. Our calculations are not self-consistent which only slightly changes the values of the matrix elements used here, but should not affect our conclusions in any essential manner. Self-consistent calculations,[8] on the other hand, are useful for obtaining accurate electronic charge densities.

The organization of the rest of the paper is as follows. In Sec. II, we briefly review the BOM and show how one can calculate various bulk properties, such as the valence-band structure and the photoelectric threshold of semiconductors. The energy matrix elements determined in this section are essential for the calculation of surface electronic structure of these semiconductors. In Sec. III, we show how one can adopt the model to the surface studies. Here we also give a very simple description of the intrinsic surface states as a prelude to our detailed calculations presented in Sec. IV. We devote Sec. IV to the discussion of our results for the electronic structure of the (111) surface of semiconductors. Silicon is examined in great detail and the results are compared with experiments. Various features in angular-resolved photoemission studies[21] are successfully explained. The electronic structure of ideal Ge (111) and diamond (111) surfaces is also studied. In order to investigate the aspects of the (111) surface electronic structure of semiconductors in the sphalerite

structure, especially to see the effect of the asymmetry in bond orbitals, a study of both cation and anion (111) surfaces of AlP is included. The general trends obtained from our study (based on a number of semiconductors) are briefly summarized at the end. Finally, we close with our conclusion in Sec. V.

II. BOM FOR BULK ELECTRONIC PROPERTIES AND THE PHOTOELECTRIC THRESHOLD

A variety of approaches for determining the energy-band structure of semiconductors have, in the past, been developed wherein one concentrates on a particular material and performs detailed calculations.[22] However, the simple chemical bond concept[23,24] has been useful in understanding whole series of properties of these solids in a systematic way. The change in the ionic character of the purely covalent bond as one goes from an elemental semiconductor to the compound (i.e., increasing asymmetry of the bond), has been shown to correlate many properties including the electronic energy structure.[18,19,24] The BOM[18,19] employs similar concepts, and starts from the anion sp^3 hybrid orbital $|h^a\rangle$ and the cation sp^3 hybrid orbital, $|h^c\rangle$ directed along the same bond [see Fig. 1(a)]. Two energy parameters describe the intrabond interactions. The covalent energy,[18,25] V_2 is the measure of the hopping from the anion to the cation

$$V_2 = -\langle h^a|H|h^c\rangle/(1-S^2). \tag{1}$$

The polar energy[18,25] V_3 reflects the tendency of the electrons to move from the cation to the anion

$$V_3 = (\langle h^c|H|h^c\rangle - \langle h^a|H|h^a\rangle)/(1-S^2)^{1/2}. \tag{2}$$

Here, the overlap of two hybrid orbitals, $S \equiv \langle h^a|h^c\rangle$ is calculated[19] to be ~ 0.5. Note that in elemental semiconductors, $|h^a\rangle \equiv |h^c\rangle$, therefore, $V_3 = 0$, and the polarity of the bond[18]

$$\alpha_p \equiv V_3/(V_2^2+V_3^2)^{1/2} \tag{3}$$

vanishes. The values of these energy parameters were obtained[18] from the dielectric properties of these solids. The bond orbital $|b_i\rangle$ directed along ith tetrahedral direction is constructed from the linear combination of $|h^a\rangle$ and $|h^c\rangle$ as was first done by Coulson and co-workers[25] [see Fig. 1(b)]

$$|b_i\rangle = u_a|h_i^a\rangle + u_c|h_i^c\rangle. \tag{4}$$

The coefficients u_a and u_c are determined from the minimized bonding energy[18]

$$V_b = -(V_3^2+V_2^2)^{1/2} + SV_2. \tag{5}$$

Note that $u_c = u_a = [2(1+S)]^{-1/2}$ for an elemental semiconductor. As is usual in the tight-binding method, the Bloch sums are now formed in terms of bond orbitals

$$|X_i(\vec{k},\vec{r})\rangle = \frac{1}{\sqrt{N}}\sum_j e^{i\vec{k}\cdot\vec{R}_j}|b_i(\vec{r}-\vec{R}_j)\rangle, \quad i=1,\ldots,4. \tag{6}$$

Here $\vec{R}_j$ denotes the translational vectors of the fcc lattice. Customary variational arguments lead to the secular equation

$$(\underline{H}-E\underline{I})\vec{a} = 0, \tag{7}$$

where the interactions of the neighboring bond orbitals, i.e., the elements of $\underline{H}$, are expressed in terms of four energy parameters[19,26]

$$\begin{aligned} A &= -\langle b_i(\vec{r})|H|b_j(\vec{r})\rangle \quad \text{(anion site, } i\neq j\text{)},\\ C &= -\langle b_i(\vec{r})|H|b_j(\vec{r})\rangle \quad \text{(cation site, } i\neq j\text{)},\\ V_4 &= \langle b_i(\vec{r})|H|b_i(\vec{r}-\vec{R}_l)\rangle,\\ D &= -\langle b_i(\vec{r})|H|b_j(\vec{r}-\vec{R}_l)\rangle, \quad i\neq j, \end{aligned} \tag{8}$$

where $\vec{R}_l$ denotes the first-neighbor translational vectors of the fcc lattice. Note that for elemental semiconductors, $A = C$ and $2A$ or $2C$ is denoted by V_1.[18] Through the interactions described in Eq. (8), the single level of the bond energy broadens into the valence band as shown in Fig. 1(c). In Table I, the energy eigenvalues of the secular matrix in Eq. (7) are given for high symmetry

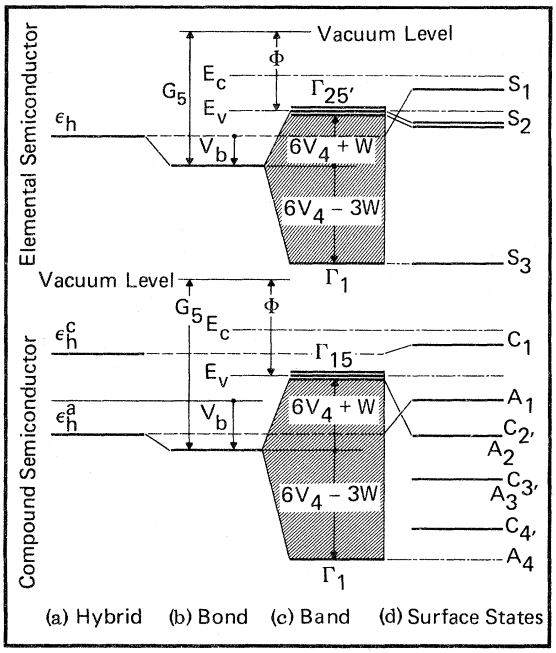

FIG. 1. Schematic description of the bulk and surface states from the bond-orbital point of view. (a) Energies of starting hybrid orbitals. (b) Bond forming. (c) Broadening into the valence band. (d) Producing certain surface states due the effect of the surface. (The symbols are explained in the text.)

TABLE I. Energy eigenvalues of the bulk electronic states at high symmetry points of the BZ. (In elemental semiconductors $X_5 \rightarrow X_4$, $X_3 \rightarrow X_1$, $\Gamma_{15}' \rightarrow \Gamma_{25}'$, $L_3 \rightarrow L_3'$, and $L_1 \rightarrow L_2'$.)

$$E(\Gamma_{15}) = 0$$
$$E(\Gamma_1) = -4W^{a}$$
$$E(X_5) = -8(D + V_4)$$
$$E(X_3) = -4(C + 2V_4)$$
$$E(X_1) = -4(A + 2V_4)$$
$$E(L_3) = -4(D + V_4)$$
$$E(L_1) \cong -(8V_4 + 2W) + 2[A^2 + C^2 - AC - 2V_4(A + C)]^{1/2}$$
$$E(L_1) \cong -(8V_4 + 2W) - 2[A^2 + C^2 - AC - 2V_4(A + C)]^{1/2}$$

[a] $W = A + C + 4D$ [see Eq. (11)].

points in terms of A, C, V_4, and D.

Since no explicit form for the hybrid orbitals is used, one has to determine A, C, V_4, and D from the experimental data or from the realistic band structure calculations. In Ref. 19, the fit to the Herman and co-workers[22] orthogonalized-plane-wave (OPW) band models has been provided by using the following relations:

$$\begin{aligned} A &= -\tfrac{1}{16}[3E(X_1) - 2E(X_5) - E(X_3) + E(\Gamma_1)], \\ C &= -\tfrac{1}{16}[3E(X_3) - 2E(X_5) - E(X_1) + E(\Gamma_1)], \\ V_4 &= -\tfrac{1}{32}[E(X_3) + E(X_1) - E(\Gamma_1) + 2E(X_5)], \\ D &= -\tfrac{1}{32}[2E(X_5) - E(X_3) - E(X_1) + E(\Gamma_1)]. \end{aligned} \tag{9}$$

The values of these parameters along with V_2, V_3, and α_p are listed in Table II. It is seen from Fig. 2 that one can obtain a fairly good description of the valence-band structure and of the densities of states in terms of only a few parameters. In addition, the model has been very successful in exploring various properties of semiconductors.[18,19]

Next, let us study the photoelectric threshold of semiconductors, which is of considerable importance in determining the energy matrix elements used in the calculation of the surface electronic energy structure. We therefore concentrate on the secular matrix (whose elements are described in the Appendix) at the Γ point. By taking the bond energy as a reference, we obtain

$$\underline{H} - E\underline{I} = \begin{pmatrix} 6V_4 - E & -W & -W & -W \\ -W & 6V_4 - E & -W & -W \\ -W & -W & 6V_4 - E & -W \\ -W & -W & -W & 6V_4 - E \end{pmatrix}, \tag{10}$$

where the band-broadening energy is

$$W = A + C + 4D. \tag{11}$$

This is a standard matrix whose eigenvalues are

$$\begin{aligned} E(\Gamma_{25}') &= 6V_4 + W \quad \text{(triplet)}, \\ E(\Gamma_1) &= 6V_4 - 3W \quad \text{(singlet)}. \end{aligned} \tag{12}$$

By adding the absolute bond energy to the triplet energy one is able to obtain the absolute energy of

TABLE II. Covalent and polar energy, polarity, and bulk energy parameters obtained from OPW band models. V_2, V_3, and α_p are taken from Ref. 18.

Semiconductor	V_2 (eV)	V_3 (eV)	α_p	A[a] (eV)	C (eV)	V_4 (eV)	D (eV)
C	6.10	0	0	2.20	2.20	0.47	0.24
Si	2.20	0	0	1.34	1.34	0.28	0.06
Ge	2.15	0	0	1.46	1.46	0.32	0.03
α-Sn	1.76	0	0	1.27	1.27	.29	0.01
AlP	2.20	1.18	0.47	1.74	0.84	0.20	0.03
AlAs	2.18	1.06	0.44	1.93	0.81	0.22	0.03
AlSb	1.97	1.26	0.54	1.49	0.91	0.23	0.03
GaP	2.18	1.33	0.52	1.80	1.03	0.25	0.03
GaAs	2.15	1.21	0.50	2.10	0.88	0.26	0.02
GaSb	1.94	0.94	0.44	1.87	0.82	0.26	0.02
InP	1.97	1.41	0.58	2.02	0.71	0.20	0.01
InAs	1.94	1.22	0.53	2.19	0.71	0.22	0.01
InSb	1.76	1.04	0.51	1.81	0.71	0.21	0.01
ZnS	2.18	2.32	0.73	2.21	0.62	0.18	0.02
ZnSe	2.15	2.26	0.72	2.28	0.68	0.19	0.01
CdSe	1.94	2.35	0.77	2.17	0.54	0.16	0.01
CdTe	1.76	2.08	0.76	2.01	0.59	0.19	0.00
CuBr[b]	2.15	2.77	0.79	3.20	0.63	0.13	0.00

[a] In elemental semiconductors $2A = 2C = V_1$.

[b] Since no complete OPW band model is available, some of the parameters for this solid are estimated by interpolation.

the valence-band edge, which is designated as the photoelectric threshold Φ. For this purpose we use the average of anion and cation hybrid energies,[27] as shown in Fig. 1, and arrive at the result[28]

$$\Phi = -\tfrac{1}{2}(\epsilon_h^c + \epsilon_h^a) - V_b - 6V_4 - W\,, \qquad (13)$$

where V_b is given in Eq. (5). In Fig. 3, the experimentally known photoelectric thresholds[13,29,30] are compared with our predictions of Eq. (13). Small deviations from the straight line might be attributed to the different band bendings in different semiconductors. Having this brief summary of the model, we show in Sec. III how one adopts the model to the surface studies.

III. BOM FOR SURFACE ELECTRONIC PROPERTIES

The cleavage through a (111) plane intuitively implies the breaking of the bonds and the creation of dangling bonds sticking into the vacuum. In terms of the BOM, each bond orbital is broken into two dangling bonds, one associated with each surface. To accomplish this, it costs approximately the bonding energy V_b. Our calculation for Si gives 1.1 eV per dangling bond for the cleavage energy. This is in good agreement with the experimental value[31] of ~1.0 eV per dangling bond.

The surface electronic structure differs from the bulk due to the presence of these dangling bonds,

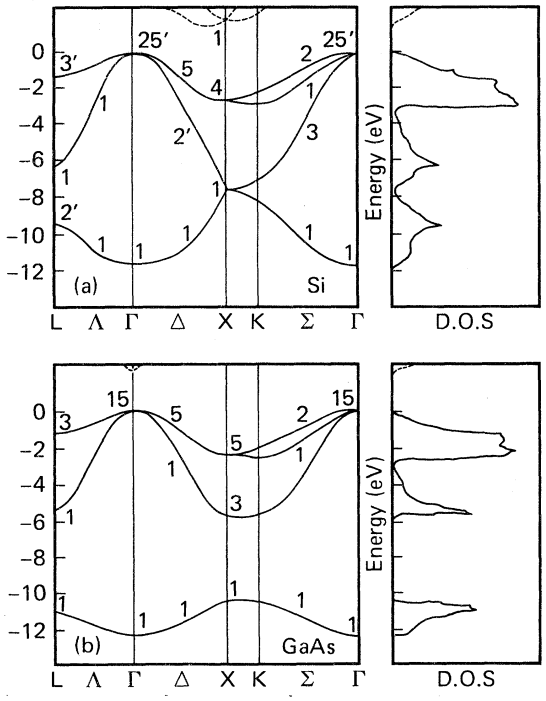

FIG. 2. Valence-band structures and corresponding densities of states calculated in terms of A, C, V_4, and D. (a) Elemental semiconductor Si. (b) Compound semiconductor GaAs.

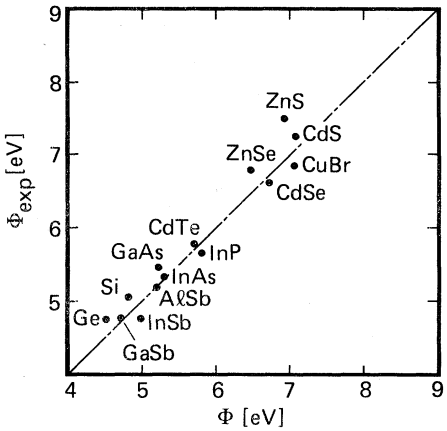

FIG. 3. Experimental photoelectric threshold Φ_{exp} vs the calculated photoelectric threshold Φ. Experimental values are taken from Refs. 29 and 30.

which destroy the translational periodicity in the direction normal to the surface. From the tight-binding point of view, the presence of the surface is taken into account through the changes of the Hamiltonian matrix elements which express the interactions of the orbitals in the top few surface layers. Away from the surface region, bulk energy parameters were used. We describe below all the energy matrix elements necessary to obtain the surface electronic energy structure of the ideal (111) surface of semiconductors.

(i) For the dangling bond energy, we have

$$G_1^{a,c} = \langle h_1^{a,c}(\vec{r}) \,|H|\, h_1^{a,c}(\vec{r}) \rangle\,; \qquad (14)$$

here the superscripts a and c stand for the anion and the cation, respectively. The symbols without superscript belong to elemental semiconductors. It should be noted that the self-energy of the dangling bond $G_1^{a,c}$ can be taken as atomic sp^3 hybrid energies (as shown in Fig. 1). Alternatively, one can calculate it by using the experimental photoelectric threshold[13,29,30] Φ and expressing all the energy states (including the intrinsic surface states) with respect to the vacuum level. According to Fig. 3 there is, however, no significant difference between the two schemes.

(ii) We have the interaction energy between the dangling bond and the back bonds

$$G_2^{a,c} = \langle h_1^{a,c}(\vec{r}) \,|H|\, b_j(\vec{r}) \rangle\,, \quad j \neq 1\,. \qquad (15)$$

(iii) Next we have the interaction energy between the dangling bond and the nearest-neighboring bond orbitals

$$\begin{aligned} G_3^{a,c} &= \langle h_1^{a,c}(\vec{r}) \,|H|\, b_1(\vec{r} - \vec{R}_l) \rangle, \\ G_4^{a,c} &= \langle h_1^{a,c}(\vec{r}) \,|H|\, b_i(\vec{r} - \vec{R}_l) \rangle, \quad i \neq 1. \end{aligned} \qquad (16)$$

(iv) We have the bond energy

$$G_5 = \langle b_i(\vec{r}) | H | b_i(\vec{r}) \rangle \ . \tag{17}$$

(v) We have the interaction energy between adjacent bond orbitals

$$G_6^{a,c} = \langle b_i(\vec{r}) | H | b_j(\vec{r}) \rangle, \quad i \neq j \ . \tag{18}$$

Here, the value of G_6 depends on what kinds of ionic site are being considered ($G_6^a = A$ and $G_6^c = C$, but for elemental semiconductors $G_6 = A = C$).

(vi) Lastly, we have the interaction between nearest neighbor bond orbitals

$$\begin{aligned} G_7 &= \langle b_i(\vec{r}) | H | b_i(\vec{r} - \vec{R}_l) \rangle \ , \\ G_8 &= \langle b_i(\vec{r}) | H | b_j(\vec{r} - \vec{R}_l) \rangle \ , \quad i \neq j \ . \end{aligned} \tag{19}$$

The equations relating these matrix elements to polar, covalent, and band-broadening energies are given for elemental and compound semiconductors in Table III. In Fig. 4 we schematically describe the energy parameters G_1–G_8 for an elemental semiconductor. By using these matrix elements, the semiinfinite solid is represented by a system having the two-dimensional periodicity of the surface shown in Fig. 5. The third dimension is terminated after a finite number of layers which yields a convergent electornic structure. Upon increasing the number of layers from 12 to 18, the valence-band edges and the energies of various surface states remained essentially unchanged. Even a slab containing six layers displays strikingly all the prominent peaks in the total densities of states.

Before applying our model in detail, let us illustrate the essential features of the surface states by considering only the first two layers, consisting of dangling bonds and back bonds. Taking the bond energy as the reference level, the secular matrix of this system at the center of the surface Brillioun zone (BZ) is

$$\underline{H}_s - E\,\underline{I} = \begin{pmatrix} \Delta + 4G_7 - E & -W_d & -W_d & -W_d \\ -W_d & 4G_7 - E & -W_b & -W_b \\ -W_d & -W_b & 4G_7 - E & -W_b \\ -W_d & -W_b & -W_b & 4G_7 - E \end{pmatrix} . \tag{20}$$

Here, the matrix elements for the interactions of the orbitals are different from their bulk values given in Eq. (10). They are

$$\begin{aligned} \Delta &= G_1 - G_5 - 4G_7, \\ W_d &= -(G_2 + 2G_3), \\ W_b &= -(2G_6 + 2G_8). \end{aligned} \tag{21}$$

The above secular matrix has the following eigenvalues:

$$\begin{aligned} E(S_1) &= -W_b + 4G_7 + \tfrac{1}{2}\Delta + [(W_b - \tfrac{1}{2}\Delta)^2 + 3W_d^2]^{1/2} \\ &\quad \text{(nondegenerate)}, \\ E(S_2) &= W_b + 4G_7 \\ &\quad \text{(doubly degenerate)}, \\ E(S_3) &= -W_b + 4G_7 + \tfrac{1}{2}\Delta - [(W_b - \tfrac{1}{2}\Delta)^2 + 3W_d^2]^{1/2} \\ &\quad \text{(nondegenerate)}. \end{aligned} \tag{22}$$

If the expressions given in Table III are substituted for G_1, $G_2 \cdots G_8$ in Eqs. (21) and (22), one can conclude the following. Creating the surface and therefore replacing one of the bond orbitals of the system by a dangling bond causes one of the states of the triplet $E(\Gamma_{25}')$ in Eq. (12) to be pulled up from the valence band to produce the dangling bond surface state S_1. The remaining two states in the triplet are pushed down, and create two states S_2, which resonate with bulk states. The lowest state, separates from the bulk $E(\Gamma_1)$, and produces another intrinsic surface state designated as the S_3 back bonding state. These splittings are shown schematically in Fig. 1(d). Upon relaxa-

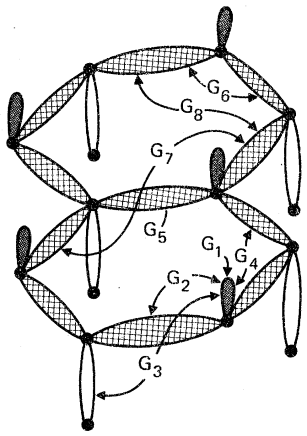

FIG. 4. Schematic description of the energy matrix elements used in the surface states calculation of an elemental semiconductor. The dotted orbitals stand for the dangling bonds. The crosshatched orbitals are the back bonds. The blank orbitals are between the second and third layers, and correspond to the orbital-5 in Fig. 5(a).

TABLE III. Equations relating the surface energy parameters to the bulk energy parameters. Note that the back bond energy differs from G_5 when the relaxation or reconstruction takes place.

Elemental semiconductor (111)	Cation-rich compound (111)	Anion-rich compound (111)
$G_1 = -(\Phi + V_b) - 6V_4 - W$, or $= \epsilon_h$	$G_1^c = \epsilon_h^c$	$G_1^a = \epsilon_h^a$
$G_2 = -V_1/2u$	$G_2^c = -C/u_c$	$G_2^a = -A/u_a$
$G_3 = V_4/u$	$G_3^c = V_4/u_c$	$G_3^a = V_4/u_a$
$G_4 = -D/u$	$G_4^c = -D/u_c$	$G_4^a = -D/u_a$
$G_5 = -(\Phi + 6V_4 + W)$	$G_5 = -(\Phi + 6V_4 + W)$	$G_5 = -(\Phi + 6V_4 + W)$
$G_6 = -\frac{1}{2}V_1$	$G_6^c = -C$	$G_6^a = -A$
$G_7 = V_4$	$G_7 = V_4$	$G_7 = V_4$
$G_8 = -D$	$G_8 = -D$	$G_8 = -D$

tion, G_1 and G_2 increase, but the bond energy G_5 of the back bonds decreases. As a result, the S_1 state rises and S_2 becomes more prominent. In the case of the reconstruction we have two different dangling-back bond groups which are associated with raised and lowered atoms in the (2×1) surface unit cell [see Fig. 5(b)]. For each group, Δ, G_2 and G_5, are different. Therefore, we expect to have two surface-state bands one corresponding to each group. In Sec. IV, we study the surface states by including many layers. Additional surface states localized in deeper layers will thus be obtained. The dispersions of the surface state bands and the total densities of states will be calculated.

IV. SURFACE STATES

A. Ideal Si(111) - (1 × 1)

By using the energy matrix elements listed in Table III, we calculated the total density of states of ideal Si(111) - (1×1). The distribution shown in Fig. 6 is obtained from 86 000 energy eigenvalues of a 12 layer slab. The shape of the curve resembles the bulk density of states presented in Fig. 3. Additional structure due to the effect of the surface is clearly evident. Before discussing the nature of these surface states, we would like to divide them into two classes: (i) *Universal surface*

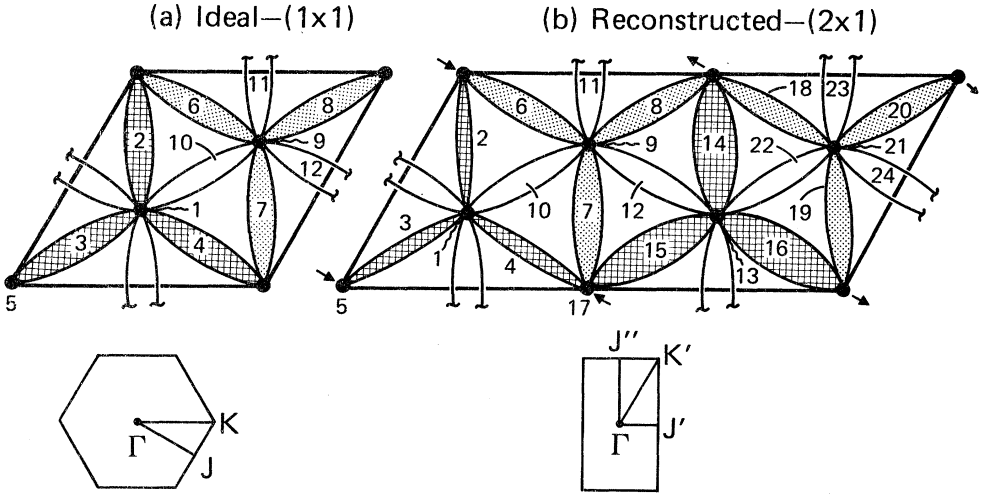

FIG. 5. Unit cells and corresponding Brillouin zones for (a) ideal Si(111)-(1×1) and (b) reconstructed Si(111)-(2×1). Here numbers denote various type of orbitals in one unit cell. In (a) 1-dangling bond, 2, 3, and 4=back bonds, 5=bond orbital between second and third layers, 6, 7, and 8=bond orbitals between third and fourth layers, etc. In (b) 1 =raised dangling bond, 13=lowered dangling bond, 2, 3 and 4=back bonds of raised dangling bond, 14, 15 and 16=back bonds of lowered dangling bonds, etc.

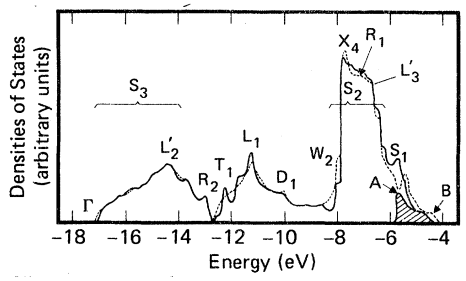

FIG. 6. Total densities of states for ideal Si(111) (solid lines). The energy parameters used were: $G_1 = -8.50$ eV, $G_2 = -2.32$ eV, $G_3 = 0.50$ eV, $G_4 = -0.08$ eV, $G_5 = -9.60$ eV, $G_6 = -1.34$ eV, $G_7 = 0.28$ eV, $G_8 = -0.06$ eV. (The crosshatched area corresponds to the energy distribution of the dangling bond surface state, S_1.) Dashed lines show the total densities of states for relaxed Si(111). Energy parameters are: $G_1 = -7.50$ eV, $G_2 = -2.10$ eV, for back bonds $G_5 = -9.90$ eV. The others are unchanged. L_2', L_1, W_2, X_4, and L_3' denote the periodic bulk-like structure.

states have associated with them a band structure and their charge is localized in the top two layers; (ii) *Regional surface states* are found in some special regions of the surface BZ and their charge is localized in deeper layers. In the light of this classification, let us now examine the electronic structure of ideal Si(111).

First, self-consistent study[8] reported three universal surface states for the relaxed Si(111) $-(1\times1)$: the dangling bond surface state S_1, the upper back bonding states S_2, and the lower back bonding state S_3. In Fig. 6, one sees a peak near the edge of the valence band corresponding to the dangling bond surface state S_1. This half-filled surface-state band has a total width of 1.4 eV, but more important, it overlaps both the valence band and the energy gap. As will be discussed in detail later, the chemisorption of hydrogen causes the surface state S_1 to disappear (see Fig. 11). By taking the difference of the distributions with and without hydrogen, one obtains the crosshatched area, which corresponds to the energy distribution of S_1. This asymmetric distribution exhibits a strong peak A, which lies in the valence band. The shape and the width of S_1 is in good qualitative agreement with the experimental results,[15,16] although their data probably correspond to a reconstructed surface. As will be seen below, our reconstructed surface calculations improve the agreement further. Appelbaum and Hamann[8] find dangling bond surface states totally lying in the gap. By analyzing the state vectors and the local densities of states,[32] we also find another intrinsic surface state at the bottom of the valence band, which corresponds mostly to the bonding combination of s-like states at the top two layers. This is the lower back bonding state S_3. As shown in Sec. III, the upper back bonding states S_2 corresponding to a bonding combination of p-like states are not well localized. In Fig. 7, we are therefore able to present the band structures for S_1 and S_3. Note that the shape of the S_1 band is similar to that reported by Pandey and Phillips.[9]

Having discussed the universal surface states of ideal Si(111) let us consider the regional surface states.[33] As stated earlier, no band structure can be associated with them because they arise only at some special points, of the surface BZ as also pointed out elsewhere.[10-11,32,34] The state called R_2 appears at the corner K, and has its charge localized especially between the second and third layer (around the orbital designated as 5 in Fig. 5). This state produces the peak R_2 in Fig. 6. The states contributing to the peak T_1 in Fig. 6 arises around the J point. Similar to R_2, T_1 also has its charge localized around the orbital-5. The states at the peak, D_1, consist of the bond orbitals around the twelfth layer. This peak is an artifact of the model consisting of a finite number of layers.

In Fig. 8, we present the total densities of states for ideal diamond and Ge(111). Due to stronger interaction between the bond orbitals in diamond (see Table II) one expects a wider dangling bond surface band than Si and Ge. Dispersion curves for diamond are similar to Si and are not shown. Pugh[4] has calculated S_1 dispersion for diamond and has the opposite sign compared to ours and

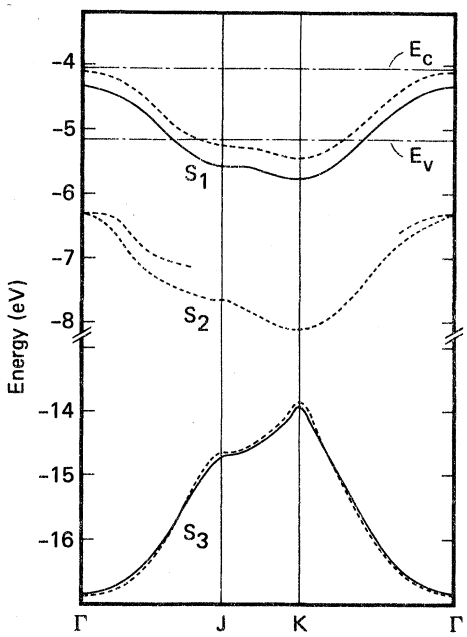

FIG. 7. Energy-band structure of the universal surface states for the ideal Si(111) (solid line) and the relaxed Si(111) (dashed lines).

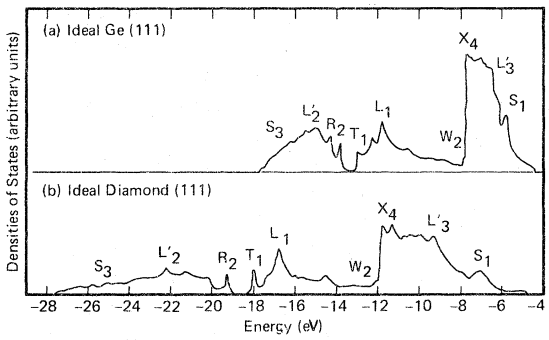

FIG. 8. Total densities of states for (a) ideal Ge(111). The energy parameters are: $G_1=-8.80$ eV, $G_2=-2.52$ eV, $G_3=0.56$ eV, $G_4=-0.05$ eV, $G_5=-9.77$ eV, $G_6=-1.46$ eV, $G_7=0.32$ eV, $G_8=-0.03$ eV; (b) ideal diamond (111). The energy parameters are: $G_1=-11.11$ eV, $G_2=-3.80$ eV, $G_3=0.82$ eV, $G_4=-0.41$ eV, $G_5=-14.16$ eV, $G_6=-2.20$ eV, $G_7=0.47$ eV, $G_8=-0.24$ eV.

other similar studies.[8,9]

B. Relaxed Si(111) - (1 × 1)

The relaxation model,[8] in which the surface atoms are rigidly moved inwards by 0.33 Å, is not an equilibrium state for the surface. This model is considered here only for the purpose of comparison with various other theoretical studies.[8,9] Relaxation affects the matrix elements G_1–G_5. New matrix elements can be expressed in terms of the relaxation distance and the BOM energy parameters.[18,19] When the surface atoms relax inwards, the orthogonality of the four hybrid orbitals (one dangling bond, and the three back bonds) imposes that the p_z contribution in the dangling bond Δp_z and the s contribution in the back bonds Δs increase

$$\Delta p_z = \left(\frac{(1-3\eta^2)}{(1-\eta^2)}\right)^{1/2} - \frac{3}{2}\,, \qquad \Delta s = \left(\frac{(1-3\eta^2)}{(3-3\eta^2)}\right)^{1/2} - \frac{1}{2}\,, \tag{23}$$

where η is the cosine of the angle between the dangling bond and the back bonds, and can be related to the relaxation distance. In this way the dangling bond energy G_1 rises. Increasing s contribution Δs generates a polar energy V_3 for the back bonds and consequently the charge is transferred from the second layer to the surface. Since the covalent energy V_2 is inversely proportional to the bond length[35] ($V_2 \propto d^{-n}$), V_2 also increases. As a result, the bond energy G_5, is lowered. The change in G_2 is determined by two competing factors. The decreasing overlap between the dangling bond and the back bonds due to the angular distortion, and the increasing overlap due to the charge transfer from the second layer to the first layer. As a result of the combined effect G_2 also increases. The changes in the energy parameters G_3 and G_4 due to the relaxation have negligible effects.

The total density of state for the relaxed Si(111) surface is shown in Fig. 6 by the dashed curve. Note that the energy corresponding to the peak S_1 rises in the energy gap, but the strong peak A still lies in the valence band. The weak shoulder of S_1 of the ideal Si(111) becomes prominent[32] which is denoted as B in Fig. 6. The upper back bonding states S_2 become localized. They are doubly degenerate at the Γ point. However, if one goes away from the center of the zone, one of the states delocalizes. The other continues to be a back bonding state with a small mixing from deeper orbitals. The width of the corresponding band is 1.8 eV. The lowest state for any surface wave vector $\vec{k}_s$ is always a back bonding state S_3 in both relaxed and unrelaxed systems. The band structure corresponding to these three universal surface states of relaxed Si(111) – (1×1) is given in Fig. 7 by dashed lines.

Now let us examine the corner K of the surface BZ. The state R_1, which has charge localized between the second and third layers (orbital-5), and arises only at the K point, as a result of the surface relaxation. Therefore, it is a regional surface state. The surface state designated R_2 is not any different than the R_2 state of ideal Si(111), but it localizes more upon relaxation. The peak T_1 of ideal Si(111) is smoothed out in the total density of states.

C. Reconstructed Si(111) - (2 × 1)

It is known[36] that the (111) surface of semiconductors reconstructs after cleavage in ultrahigh vacuum at the room temperature. Therefore, calculation on this reconstructed surface is more meaningful for comparison with the experimental data.

Here, we use Haneman's model[36] of (2×1) reconstruction of Si(111). Such a model has been used successfully in the past for interpreting the LEED (low-energy-electron diffraction) and EPR data.[36] In particular, we show that if we take the lattice displacements as given by Haneman, then the (2×1) reconstruction still does not produce an insulating state. It is interesting to note that Tosatti and Anderson[37] were not able to predict the (2×1) reconstruction strictly based on the theory of metal-insulator transition. The effect of the reconstruction is considered in terms of two different sets of energy matrix elements describing the interactions of the dangling bond and the back bonds. These are G_1^R, G_2^R, G_5^R for raised surface

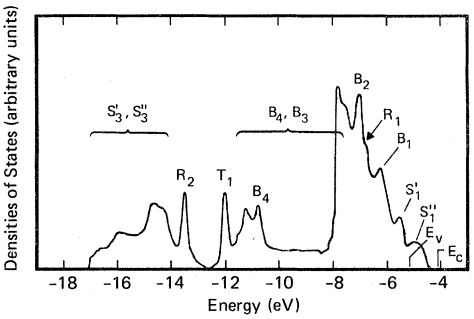

FIG. 9. Calculated total densities of states for Si(111) $-(2\times1)$. The energy parameters are: $G_1^R=-9.42$ eV, $G_2^R=-2.20$ eV, $G_5^R=-9.45$ eV, $G_1^L=-8.06$ eV, $G_2^L=-2.24$ eV, $G_5^L=-9.70$ eV. Other parameters are same as in Fig. 6.

atoms, whose dangling bonds become more s-like. The other set, G_1^L, G_2^L, G_5^L, are for the lowered atoms, whose dangling bonds develop more p character in contrast to the raised atoms. These new matrix elements are calculated by following the arguments presented in Sec. IV B, rather than making empirical adjustments. It should be appreciated that no further parametrization of the energy matrix elements is necessary.

The total density of states for Si(111) $-(2\times1)$ calculated using the Haneman's model is shown in Fig. 9. The most significant effect of this (2×1) reconstruction on the surface electronic structure is to split S_1 of Si(111)$-(1\times1)$ into two peaks S_1' and S_1'' separated by about 0.6 eV. Such a splitting was first reported by Batra and Ciraci[12] using cluster model calculations. A similar splitting has also been found using pseudopotential[34] models. The back-bonding state near the top of the valence band (so called S_2) splits into four resonating back bonding states B_1, B_2, B_3, and B_4. The states contributing to the peak B_1 are strongly localized at J' (see Fig. 5). B_4, which also has a considerable amount of charge at the third layer, forms a band from -10.6 to -11.5 eV. Also, the back-bonding state near the bottom of the valence band (so called S_3) splits into two distinct bands S_3' and S_3''. The surface states R_2, R_1, and T_1 of Si(111) $-(2\times1)$ have similar features as in the ideal and relaxed Si(111), because their charges localized between the second and third layers are not affected by the reconstruction.

All these surface states calculated for the (2×1) reconstructed Si(111) are compared with various experimental measurements in Table IV. Calculated peak positions are obtained from the total and local[32] densities of states. Rowe *et al.*[38] associated the peak at 2.4 eV below the valence band edge with the emission from the first back-bonding state. However, our analysis on the local[32] densities of states suggests that this peak arises from the closely lying R_1, B_1, and B_2 states. The comparison of distributions presented in Figs. 6 and 11 also suggests that the state observed at 8.6 eV below the valence-band edge is due to the peak R_2.

In Fig. 10, we plot the band structure for the states S_1', S_1'', B_1, S_3', and S_3'' calculated using Haneman's reconstruction parameters. The upper band S_1'' has mostly p_z-orbital character and overlaps with the bulk valence band. Bulk electrons from Γ_{25}' can lower their energy by flowing to S_1''. However, as pointed out by Tosatti and Anderson,[37] strong electrostatic forces build up rapidly and pin the Fermi level slightly near the valence-band edge. The energy of S_1'' should thus

TABLE IV. Comparison of experimentally observed surface states on cleaved Si(111) with the results of the present study. Energies are measured relative to the valence-band edge.

Surface states for Si(111)-(2×1)	Peak positions in the present calculation (eV)	Experiment (eV)
S_1'	-0.4	-0.45,[a] -0.6,[b] -0.5,[c] -0.5,[d] ±0.2
B_1	-1.0 -1.5	
R_1	-1.7	
B_2	-1.8	-2.4 ± 0.2[d]
B_4	-5.6	
T_1	-6.8	
R_2	-8.3	-8.6 ± 0.2[d]
S_3', S_3''	-11.7	-11.7 eV,[c] -11.3 ± 0.4,[d] -13.5 ± 0.4[d,e]

[a] Reference 15.
[b] Reference 16.
[c] Reference 17.
[d] Reference 38.
[e] This state ~1.5 eV below the bottom of the valence-band edge probably arises due to the surface roughening.

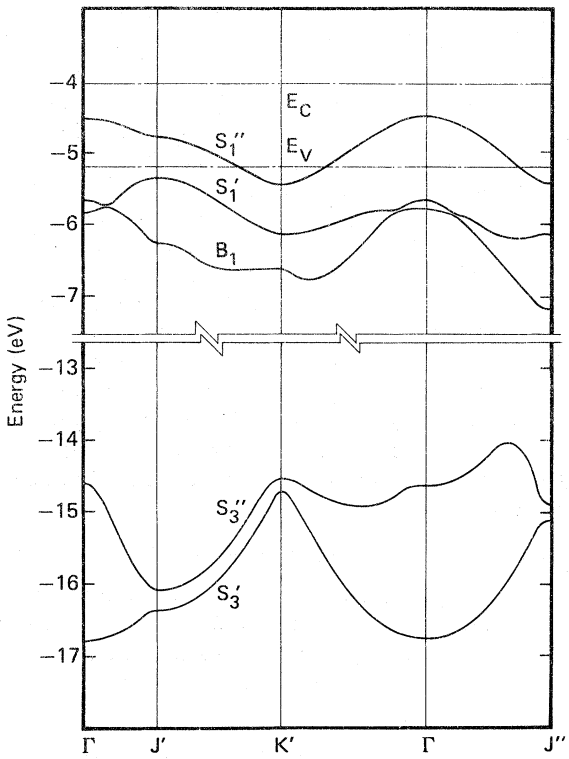

FIG. 10. Energy-band structure of the universal surface states for the Si(111)-(2×1).

be slightly raised compared to what we have shown, but it still predicts a two-dimensional metal as shown earlier.[12] It should be noted, however, that a slight extension of Haneman's model of the (2×1) reconstruction[40] (where the inward going atoms are further lowered) gives a superlattice energy gap,[39] keeping the other surface-related energy bands practically unchanged. The lower dangling bond surface band S_1' has considerable orbital-s character, and an appreciable contribution from the back bonds. It lies completely in the valence band. The top back bonding band B_1 hybridizes with S_1' along certain directions of the surface BZ, as shown in Fig. 10. This character of S_1' and B_1 states associated with the raised atoms is important for interpreting the recent angular-resolved ultraviolet-photoemission-spectroscopy [UPS(Ω)] experiment[21] for cleaved Si(111).

In UPS(Ω), Rowe *et al.*[21] sampled the $\Gamma - K'$ direction in the surface BZ by using a photon energy of 10.2 eV and fixing φ in a plane containing the dangling bond and one of the back bonds. The surface state peak observed at −1.15 eV below E_F (~ −0.8 eV below E_v) at $\theta = 25°$ can be identified with the emission from the region where S_1' and B_1 are hybridized. From the dispersion of bands in Fig. 10 for low values of $\theta (\leq 35°)$ one expects a single intense peak due to the high density of states around the Γ point (~ −0.7 eV below E_v) as indeed observed experimentally.[21] Furthermore, this peak is present for all values of φ with varying intensity. As one goes away from the center point towards K', B_1, and S_1' have different dispersions. Consequently, the original peak should split for higher values of θ. Our results also suggest that the low-binding peak (due to S_1') should be less intense[41] than the high-binding energy peak (due to B_1) because of a high density of states around B_1, and should be almost flat for higher $\vec{k}_s$ values. Experimentally, this low-binding energy peak appears as a shoulder at $\theta \simeq 40°$. The peak observed in the angular-averaged spectra[15–17,21] near the top of the valence band is due to S_1' (see Fig. 9). We are also able to explain quite simply the anisotropic emission from the surface state band by recalling that S_1' has an appreciable contribution from the back bonds.

It is important to point out that there are three back bond directions which can define the $\varphi = 0$ plane. However, due to the nature of the (2×1) reconstruction only, two of these are equivalent. The plane $\varphi = 0$, including one of these back bonds, contains the $\Gamma - K'$ direction. The unequivalent bond lies in the plane containing the $\Gamma - J'$ direction. Dispersions for various bands along both of these directions are shown in Fig. 10.

D. Chemisorption of hydrogen on Si(111) - (1 × 1)

Next, we briefly discuss the chemisorption of hydrogen on the ideal Si(111) surface. Hydrogen chemisorption is important, because it removes the intrinsic surface states of the reconstructed surfaces. Hence, it allows the indirect observation of the surface states as well as the reconstruction mechanism.[17] Here, one hydrogen atom is considered to be chemisorbed on each dangling bond. Therefore, the charge of the dangling bond is transferred to the hydrogen side, and the Si–H bond is formed. The energy of the Si–H bond is taken from the results of cluster model calculations using the self-consistent field-statistical exchange-scattering wave method.[12] The corresponding energy distribution is shown in Fig. 11. A comparison of Fig. 6 and Fig. 11 reveals that the hydrogen chemisorption removes the dangling bond and back bonding surface states, and yields two peaks, 2.3 and 5.3 eV below the valence band. In addition the saturation of the dangling bonds through hydrogen attachment depletes the states corresponding to T_1, R_1, and R_2 and slightly increases the photoelectric threshold. As shown in Fig. 11(b), our results are in agreement with the photoemission spectroscopy data of Rowe *et al.*[17,38] However, they were not able to resolve the upper peak at 2.3 eV below the valence-band edge. The

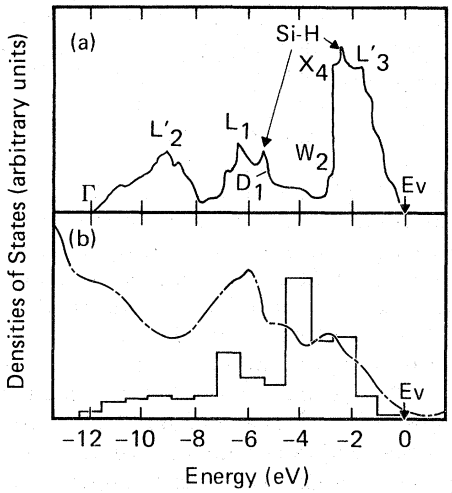

FIG. 11. (a) Calculated densities of states for hydrogen chemisorbed on ideal Si(111). (b) UPS data for clean low-step-density surface after adsorption of ~1 monolayer of atomic hydrogen (dash-dotted curve reproduced from Ref. 38). The local density of states on the hydrogen atom shown by histograms (reproduced from Ref. 42). Energies are measured relative to the valence-band edge.

local density of states on the chemisorbed hydrogen atom reported by Appelbaum and Hamann[42] is also shown in Fig. 11(b) for comparison.

E. Intrinsic surface states of compound semiconductors

Thus, far, we have studied the electronic energy structure of the (111) surface of the elemental semiconductors. Let us now consider the compound semiconductors. It has been known that the polarity α_p of the bond is the most prominent factor in correlating electronic, as well as many other properties of these materials. It is interesting to investigate similar correlations for the surface electronic structure. Unfortunately, there is not much known about their atomic arrangement for the (111) surface. Therefore, our study, based on the ideal (111) surfaces of a number of compound semiconductors, will be exemplified by presenting the results for the ideal AlP. A few important conclusions drawn from this study are summarized.

In compounds the (111) surface presents a special case where only cation or anion atoms can lie on the (111) surface. Here we separately consider both anion and cation (111) surfaces in their ideal configuration:

1. Cation-(111) surface of AlP

In this case,[43] the dangling bond surface state C_1 corresponding to the cation atom lies in the energy gap [Fig. 12(a)]. The back bonding surface states C_2 correspond to S_2 of the elemental semiconductors and are localized at the top two layers. They are doubly degenerate at the Γ point (−6.9 eV). One of these states continues to be localized at all points of the surface BZ, and has a 1.4-eV bandwidth. The other state is delocalized. We found two other surface states which are localized at the second and third layers. The upper one C_3 is located around the upper edge of the valence band gap. They are delocalized at the center of the surface BZ, but become localized at the J point. The fourth state C_4 is at the lower edge of the band gap and overlaps appreciably with the band gap. This state is prominently localized at the K corner. It is interesting to note that one is able to find a state of energy −7.0 eV, which only appears at the K corner. It has its charge localized at the third layer similar to the elemental semiconductor.

2. Anion-(111) surface of AlP

In Fig. 12(b), the total density of states corresponding to this surface is shown. Note that it has similar features as the cation surface. However, in this case the A_1 state is buried in the va-

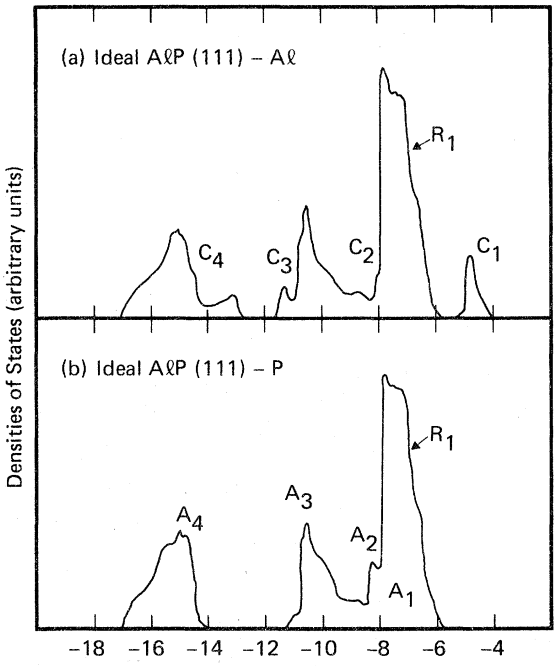

FIG. 12. Total densities of states for a compound semiconductor (a) ideal AlP(111), Al atoms are located at the surface: Corresponding energy parameters are: $G_1^c = -6.17$ eV, $G_2^c = -1.63$ eV, $G_3^c = 0.39$ eV, $G_4^c = -0.08$ eV, $G_5 = -9.75$ eV, $G_6^c = -0.84$ eV, $G_6^a = -1.74$ eV, $G_7 = 0.20$ eV, $G_8 = -0.04$ eV. (b) ideal AlP(111), P atoms are located at the surface. Energy parameters are: $G_1^a = -10.53$ eV, $G_2^a = -2.03$ eV, $G_3^a = 0.23$ eV, $G_4^a = -0.05$ eV, $G_5 = -9.75$ eV, $G_6^a = -1.74$ eV, $G_6^c = -0.84$ eV, $G_7 = 0.20$ eV, $G_8 = -0.04$ eV.

lence band and delocalized.

The following general trends in the (111) surface states of the compound semiconductors can be noted [see Fig. 1(d)]. We find that with increasing polarity α_p: (i) C_1 rises in the energy gap and becomes more flat, (ii) A_1 lowers in the valence band, and (iii) C_3, C_4 and A_3, A_4 become more localized.

V. CONCLUSION

The BOM can be used for bulk as well as surface studies. Bulk properties can be calculated in terms of four energy parameters obtained from realistic band structure calculations. One can then meaningfully investigate the surface electronic structure, relaxation, and reconstruction without invoking any further adjustable parameters. From a successful description of the surface state obtained using the BOM, we are hopeful that this method may be useful for studying chemisorption and other surface related problems.

ACKNOWLEDGMENTS

We wish to acknowledge useful discussions with Dr. P. S. Bagus, Dr. F. Herman, Dr. I. Miller, and Dr. H. F. Winters. The continuing support and encouragement of Dr. E. Kay is highly appreciated.

APPENDIX

Here we present the elements of the BOM Hamiltonian matrix $\underline{H}$ in Eq. (7):

$$
\begin{aligned}
H_{11} &= 2V_4[\cos(x+y)+\cos(y+z)+\cos(x+z)],\\
H_{22} &= 2V_4[\cos(x+y)+\cos(y-z)+\cos(x-z)],\\
H_{33} &= 2V_4[\cos(x-y)+\cos(y-z)+\cos(x+z)],\\
H_{44} &= 2V_4[\cos(x-y)+\cos(y+z)+\cos(x-z)],\\
H_{12} &= -C - A\,e^{-i(x+y)} - 2D\cos z(e^{-ix}+e^{-iy}),\\
H_{13} &= -C - A\,e^{-i(x+z)} - 2D\cos y(e^{-ix}+e^{-iz}),\\
H_{14} &= -C - A\,e^{-i(y+z)} - 2D\cos x(e^{-iz}+e^{-iy}),\\
H_{23} &= -C - A\,e^{-i(z-y)} - 2D\cos x(e^{iy}+e^{-iz}),\\
H_{24} &= -C - A\,e^{-i(z-x)} - 2D\cos y(e^{iy}+e^{-iz}),\\
H_{34} &= -C - A\,e^{-i(-x+y)} - 2D\cos z(e^{ix}+e^{-iy}),
\end{aligned}
\tag{A1}
$$

where

$$x=\tfrac{1}{2}k_x a,\quad y=\tfrac{1}{2}k_y a,\quad z=\tfrac{1}{2}k_z a, \tag{A2}$$

and a is the edge of the fcc cube.

The valence band structures obtained from this simple description are shown in Fig. 2. Another advantage of using this simple description is that one can explore various features of the valence band eigenvalues, as was discussed in detail in Ref. 19.

---

*Work partially supported by NSF Grant No. DMR74 and by IBM under a joint program.

†Permanent address: Dept. of Materials Science and Engineering, Stanford University, Stanford, Calif. 94305.

[1]I. Tamm, Z. Phys. 76, 849 (1932); Phys. Z. Sowjet 1, 733 (1932).

[2]W. Shockley, Phys. Rev. 56, 317 (1939).

[3]J. Koutecky and M. Tomasek, Phys. Rev. 120, 1212 (1960); K. Hirabayaski, J. Phys. Soc. Jpn. 27, 1475 (1969).

[4]D. Pugh, Phys. Rev. Lett. 12, 390 (1964).

[5]R. O. Jones, Phys. Rev. Lett. 20, 992 (1968).

[6]S. G. Davison and L. D. Levine, Solid State Phys. 25, 1 (1970).

[7]S. Ciraci, W. A. Harrison, P. E. Gregory, W. E. Spicer, and L. F. Wagner, Bull. Am. Phys. Soc. 19, 214 (1974); P. E. Gregory, W. E. Spicer, S. Ciraci, and W. A. Harrison, Appl. Phys. Lett. 25, 511 (1974).

[8]J. A. Appelbaum and D. R. Hamann, Phys. Rev. Lett. 31, 106 (1973).

[9]K. C. Pandey and J. C. Phillips, Phys. Rev. Lett. 32, 1433 (1974).

[10]D. J. Chadi and M. L. Cohen, Phys. Rev. B 11, 732 (1975); J. D. Joannopoulos and M. L. Cohen, *ibid.* 10, 5075 (1975).

[11]S. Ciraci and I. P. Batra, Solid State Commun. 16, 1375 (1975).

[12]I. P. Batra and S. Ciraci, Phys. Rev. Lett. 34, 1337 (1975).

[13]F. G. Allen and G. W. Gobelli, Phys. Rev. 127, 150 (1962).

[14]T. E. Fischer, Surf. Sci. 10, 399 (1968); R. C. Eden, in Proceedings of the Tenth International Conference on the Physics of Semiconductors, Cambridge, Mass. (1970) (unpublished), p. 221.

[15]D. E. Eastman and W. D. Grobman, Phys. Rev. Lett. 28, 1378 (1972).

[16]L. F. Wagner and W. E. Spicer, Phys. Rev. Lett. 28, 1381 (1972).

[17]J. E. Rowe and H. Ibach, Phys. Rev. Lett. 28, 1281 (1972); Surf. Sci. 43, 481 (1974); Phys. Rev. Lett. 32, 421 (1974).

[18]W. A. Harrison, Phys. Rev. B 8, 4487 (1973); W. A. Harrison and S. Ciraci, *ibid.* 10, 1516 (1974).

[19]S. Ciraci, Ph.D. thesis (Stanford University, 1973) (unpublished). S. Ciraci, Phys. Status Solidi B 70, 689 (1975). (The study of bulk electronic properties of semiconductors is based on the Ph. D. thesis of S. Ciraci.)

[20]G. G. Hall, Philos. Mag. 43, 338 (1952).

[21]J. E. Rowe, M. M. Traum and N. V. Smith, Phys. Rev. Lett. 33, 1333 (1974).

[22]F. Herman, R. L. Kortum, C. D. Kuglin, and J. P. Van Dyke, Methods Comput. Phys. 8, 193 (1968); F. Herman, R. L. Kortum, I. B. Ortenburger and J. P. Van Dyke, ARL Technical Report (1969) (unpublished).

[23]L. Pauling, *The Nature of Chemical Bond* (Cornell U. P., Ithaca, N.Y., 1967).

[24]J. C. Phillips, Rev. Mod. Phys. 42, 317 (1970); J. C.

Phillips, *Bonds and Bands in Semiconductors* (Academic, New York, 1973).
[25]C. A. Coulson, L. B. Redei, and D. Stocker, Proc. R. Soc. Lond. 270, 357 (1962).
[26]N. J. Shevichik, J. Tejeda, and M. Cardona [Phys. Rev. B 9, 2627 (1974)] neglected the matrix D in their analysis. However, it is important in determining the total width.
[27]F. Herman and S. Skillman, *Atomic Structure Calculations* (Prentice-Hall, Englewood Cliffs, N. J., 1963).
[28]Similar analysis was done before by S. Ciraci and B. Bell, Solid State Commun. 15, 575 (1974). They considered only the interactions A and C, and obtained a consistent correlation. Here including the first-neighbor interactions V_4 and D is capable of giving the exact value.
[29]F. G. Allen and G. W. Gobellii, Phys. Rev. 127, 141 (1962); 137, A245 (1965); T. E. Fisher, *ibid.* 139, A1228 (1965); 142, 519 (1966).
[30]The photoelectric threshold of CuBr is taken from the unpublished work of S. L. Fu (Stanford University, 1973).
[31]J. J. Gilman, J. Appl. Phys. 31, 2208 (1960).
[32]I. B. Ortenburger and I. P. Batra, Bull. Am. Phys. Soc. 20, 324 (1975); I. B. Ortenburger, S. Ciraci, and I. P. Batra (unpublished).
[33]The notation in Ref. 11 was used before this distinction is made. In this paper we keep the same notation except R_1, which is used here to denote the regional surface state at the $\bar{K}$ point of the surface BZ.
[34]M. Schlüter, J. R. Chelikowsky, S. G. Louie, and M. L. Cohen, Phys. Rev. Lett. 34, 1385 (1975).
[35]M. Cardona, W. Paul, and H. Brooks, J. Phys. Chem. Solids 8, 204 (1959).
[36]D. Haneman, Phys. Rev. 119, 563 (1960); 121, 1093 (1961); 170, 705 (1968); N. R. Hansen and D. Haneman, Surf. Sci. 2, 566 (1964); A. Taloni and D. Haneman, *ibid.* 10, 215 (1968).
[37]E. Tosatti and P. W. Anderson, Solid State Commun. 14, 773 (1974); Japan J. Appl. Phys. Suppl. 2, 381 (1974).
[38]J. E. Rowe, S. B. Christman, and H. Ibach, Phys. Rev. Lett. 34, 874 (1975).
[39]G. Chiarotti, S. Nannarone, R. Pastore, and P. Chiaradia, Phys. Rev. B 4, 3398 (1971).
[40]S. Ciraci and I. P. Batra, Phys. Rev. Lett. (to be published). See also K. C. Pandey and J. C. Phillips Phys. Rev. Lett. 34, 1450 (1975); F. Yndurain and L. M. Falicov, Solid State Commun. 17, 855 (1975).
[41]The intensity, of course, is also matrix-element dependent, a fact which is being ignored in our discussion. Note also the uncertainty in determining the position of the S_1' peak from the experimental data.
[42]J. A. Appelbaum and D. R. Hamann, Phys. Rev. Lett. 34, 806 (1975).
[43]For the sake of simplicity we approximated u_a and u_c in Table III by $[(1-\alpha p)/2]^{1/2}$ and $[(1+\alpha p)/2]^{1/2}$, respectively.